

Chemical Research in Toxicology

SEPTEMBER 2004
VOLUME 17, NUMBER 9

© Copyright 2004 by the American Chemical Society

Articles

Nitrosative Guanine Deamination: Ab Initio Study of Deglycation of *N*-Protonated 5-Cyanoimino-4-oxomethylene-4,5-dihydroimidazoles

Sundeep Rayat, Zhengyu Wu, and Rainer Glaser*

Department of Chemistry, University of Missouri—Columbia, Columbia, Missouri 65211

Received February 19, 2004

Ⓜ This paper contains enhanced objects available on the Internet at <http://pubs.acs.org/journals/crtoec>.

5-Cyanoimino-4-oxomethylene-4,5-dihydroimidazoles (**1**) (R at N1) have been discussed as possible intermediates in nitrosative guanine deamination, which are formed by dediazonation and deprotonation of guaninediazonium ion. The parent system **1** (R = H) and its *N*1 derivatives **2** (R = Me) and **3** (R = MOM) are considered here. Protonation of **1–3**, respectively, may occur either at the cyano-*N* to form cations **4** (R = H), **6** (R = Me), and **8** (R = MOM) or at the imino-*N* to form cations **5** (R = H), **7** (R = Me), and **9** (R = MOM), respectively. This protonation is the first step in the acid-catalyzed water addition to form 5-cyanoimino-imidazole-4-carboxylic acid, which then leads to oxanosine. There also exists the option of a substitution reaction by water at the R group of **6–9**, and this dealkylation forms *N*-[4-(oxomethylene)-imidazol-5-yl]-carbodiimide (**10**) and *N*-[4-(oxomethylene)-imidazol-5-yl]cyanamide (**11**). In the case of DNA, the R group is a deoxyribose sugar, and attack by water leads to deglycation. To explore this reaction option, the S_N1 and S_N2 reactions of **6–9** with water were studied at the MP2/6-31G*//RHF/6-31G* and CCSD/6-31G*//RHF/6-31G* levels, with the inclusion of implicit solvation at the IPCM(MP2/6-31G*//RHF/6-31G*) level, and the electron density distributions of tautomers **1**, **10**, and **11** were analyzed. The low barriers determined for the MOM transfer show that the deglycation could occur at room temperature but that the process cannot compete with water addition.

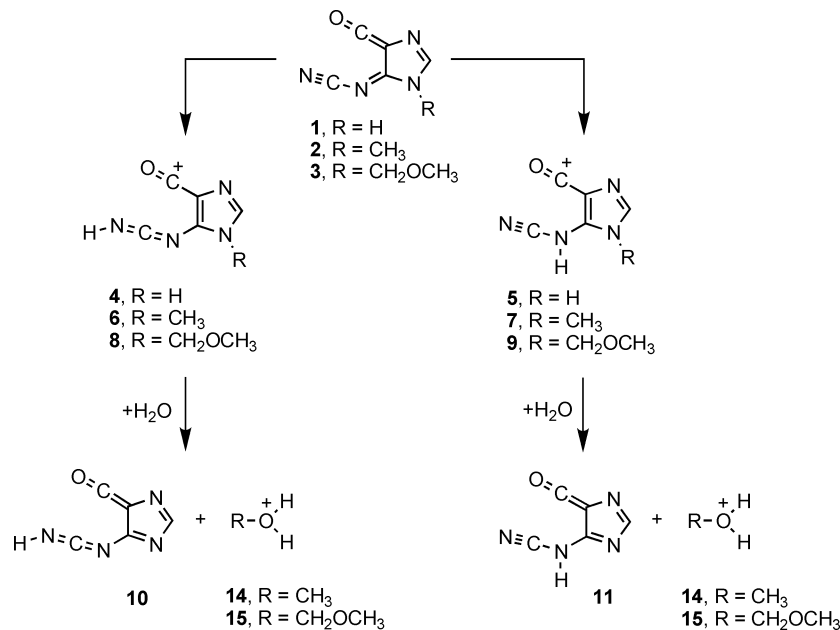
Introduction

Nitrous acid (HNO₂) causes deamination (*1–3*) and interstrand cross-link formation (*4–6*) of the DNA bases guanine, adenine, and cytosine. Nitrosative DNA base

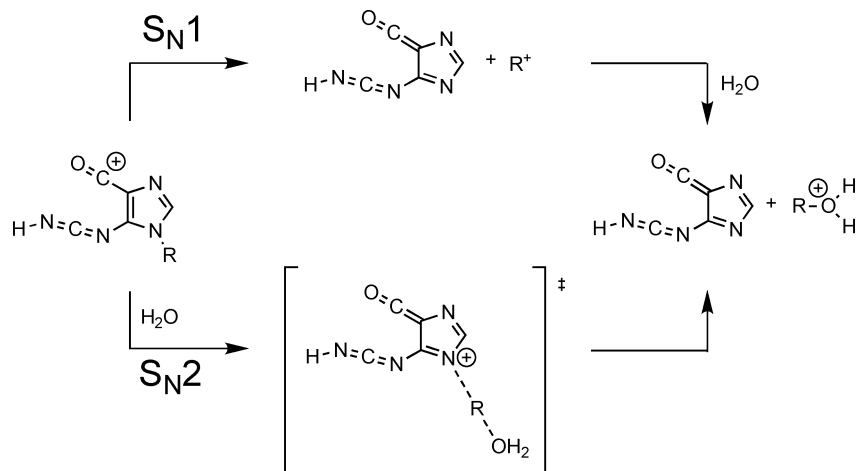
deamination represents one of the most abundant sources of endogenous DNA damage, and it constitutes a significant portion of damage in various disease states via mutagenesis and cytotoxicity. A complete understanding of the deamination chemistry is important because of the considerable dietary and environmental exposure of humans to nitrogen oxides (*7–9*). Toxicological studies

* To whom correspondence should be addressed. Fax: 573-882-2754. E-mail: glaserr@missouri.edu.

Scheme 2. Dealkylation of Cyano-*N* and Imino-*N* Protonated 5-Cyanoimino-4-oxomethylene-4,5-dihydroimidazoles (4–9)



Scheme 3. Unimolecular and Bimolecular Paths of Dealkylation Shown for the Cyano-*N* Protonated System



reaction depends on the intrinsic barrier and the reaction energy (32, 33). The intrinsic $S_{\text{N}}2$ barriers for anionic O and N nucleophiles in methyl transfer reactions are 19.5 and 29.3 kcal/mol (34, 35). In the dealkylation reaction of interest here, the nucleophile is neutral, the leaving group is protonated, and the reactive center is oxygen-substituted. While the neutrality of the nucleophile is rate retarding, it is reasonable to anticipate the other two features to be rate accelerating. Protonation improves the leaving group (36), and this effect should manifest itself to some extent even though the site of protonation is somewhat remote. Nucleoside hydrolases are characterized by the protonation of the leaving group and by the fact that they stabilize oxocarbenium ion transition states (37, 38). Similarly, the MOM group will alter the height of the intrinsic barrier as it allows the reactive center to become more like a methoxymethyl cation (39–41). Hence, it is an open question whether deglycation might occur.

Previously, we presented an ab initio study of the cyano-*N* and imino-*N* protonation of the 5-cyanoimino-4-oxomethylene-4,5-dihydroimidazole (1) (R = H) and its

*N*1 derivatives 2 (R = Me) and 3 (R = MOM) resulting in the formation of cations 4–9 (42). In this article, we discuss the thermodynamics and kinetics of the dealkylation of protonated *N*1-alkyl-5-cyanoimino-4-oxomethylene-4,5-dihydroimidazoles 2 (R = Me) and 3 (R = MOM) with water. The MOM group presents the smallest reasonable model of the sugar moiety. We consider the “deglycation” reactions for the tautomers formed by cyano-*N* (6 and 8) and imino-*N* (7 and 9) protonation of 2 and 3, respectively. The unimolecular and bimolecular hydrolyses (Scheme 3) were examined in all cases. For the bimolecular reaction, pre- and postcoordination complexes and the reaction transition state structures between them were located, and the discussion considers both the unimolecular reaction of the aggregate as well as the direct nucleophilic substitution.

Computational Methods

Potential energy surfaces were explored with Gaussian98 (43) on clusters of ES40 and ES45 Alphaservers. Geometries and frequencies were calculated with re-

Table 1. Total Energies and Thermodynamical Data^a

str	symmetry	E_{tot} (RHF) ^b	VZPE ^c	TE ^c	S ^d	NIF ^e	E_{tot} (MP2) ^b	E_{tot} (CCSD) ^b	E_{tot} (IPCM) ^b
1a	C_s	-483.108682	49.88	54.59	87.23	0	-484.527829	-484.543632	-484.594161
1b	C_s	-483.109789	49.94	54.66	87.58	0	-484.526345	-484.543419	-484.594488
6a	C_s	-522.496047	75.31	81.78	102.16	0	-524.043730	-524.069749	
7a	C_s	-522.489027	76.89	82.87	96.68	0	-524.035596	-524.065812	
8b-Sg	C_1	-636.379489	98.27	105.91	112.27	0	-638.231361	-638.269728	-638.378390
9a-Sg	C_1	-636.376461	100.01	107.26	107.76	0	-638.227860	-638.270004	-638.376739
10b	C_1	-483.090125	48.75	53.58	89.22	0	-484.512867	-484.525638	-484.567267
11a	C_s	-483.099413	49.53	54.43	89.48	0	-484.519884	-484.535475	-484.583938
11b	C_s	-483.093162	49.40	54.43	90.46	0	-484.511953	-484.528846	-484.582851
12	D_{3h}	-39.230640	21.16	22.94	44.51	0	-39.325142	-39.345464	
13	C_s	-153.204029	46.54	49.08	63.33	0	-153.618733	-153.648046	-153.73696
13'	C_s	-153.202747	46.30	48.44	60.63	1	-153.617057	-153.649596	
14	C_1	-115.338992	43.04	45.29	58.34	0	-115.644288	-115.668742	
15	C_1	-229.244328	63.36	67.78	80.26	0	-229.847332	-229.886068	-229.961837
16	C_1	-598.523161	91.39	100.03	119.49	0	-600.261498	-600.295259	
17	C_1	-598.518625	92.99	101.24	115.2	0	-600.254021	-600.292527	
18	C_1	-712.416490	114.98	124.61	129.48	0	-714.456683	-714.503372	-714.598651
19	C_1	-712.411864	116.4	125.66	123.00	0	-714.454193	-714.503691	-714.602932
20	C_1	-598.467816	93.21	100.82	113.45	0	-600.207182	-600.241285	
21	C_1	-598.447075	93.04	101.42	121.85	0	-600.177646	-600.216449	
22	C_1	-712.359020	113.82	123.80	133.43	0	-714.394075	-714.443015	-714.546620
23	C_1	-712.357306	114.12	124.35	134.97	0	-714.389211	-714.441748	-714.557066
24	C_1	-598.441503	91.00	98.97	115.59	1	-600.179506	-600.213707	
25	C_1	-598.439482	91.58	99.769	119.93	1	-600.171164	-600.210091	
26	C_1	-712.357194	112.97	122.83	135.53	1	-714.389796	-714.439207	-714.538037
27	C_1	-712.355033	114.05	123.77	130.80	1	-714.386983	-714.442531	-714.541508
H ₂ O	C_{2v}	-76.010747	14.42	16.20	44.99	0	-76.195956	-76.204968	-76.211437

^a All calculations employed the 6-31G* basis set. ^b Total energies (E_{tot}) are in hartrees. ^c Vibrational zero-point energies (VZPE) and thermal energies (TE) are in kcal/mol. ^d Entropy (S) is in cal/mol K. ^e Number of imaginary frequencies (NIF).

stricted Hartree–Fock theory in conjunction with the 6-31G* basis set (44, 45). Minima and transition state structures were characterized by the presence of zero or one imaginary mode, respectively. Better relative and reaction energies were determined with second-order Møller–Plesset perturbation theory, MP2(fc), and coupled cluster theory that considers all single and double excitations, CCSD(fc). The active space in the correlation calculations includes all valence electrons and all virtual orbitals; this choice of active space is referred to as the frozen core approximation (fc). In MP2 theory, the contributions of all excitations are approximated based on information of the RHF reference wave function. In contrast, in coupled cluster theory, the individual contributions of single and double excitations are determined variationally. The CCSD(fc) data thus are far superior as compared to the MP2(fc) data, but the improvement achieved by the use of variational instead of perturbational configuration interaction methods comes with substantially increased computer time demands. The MP2 and CCSD calculations were based on RHF/6-31G* structures: MP2/6-31G**/RHF/6-31G* and CCSD/6-31G**/RHF/6-31G*. Total energies and thermodynamic parameters are reported in Table 1, and relative energies and relative Gibbs free energies are given in Table 2. Relative Gibbs free energies based on MP2 or CCSD energies employ the RHF thermochemical data. Thermal energies were used as computed. The data in Table 2 show that there is complete qualitative agreement between the RHF, MP2, and CCSD data while there are some expected and significant quantitative differences in the reaction energies. The ΔG_{rel} values calculated at the CCSD/6-31G**/RHF/6-31G* level are discussed.

Solvation effects were examined with an implicit solvent method (46). Solvation energies were determined with the isodensity surface polarized continuum model (IPCM; 47) for water ($\epsilon = 78.39$). IPCM calculations were

carried out at the MP2/6-31G* level, and they were based on the gas phase RHF/6-31G* structures.

Electronic structures were analyzed with natural population analysis (48–50) of the correlated electron densities determined at the MP2/6-31G**/RHF/6-31G* level and with the inclusion of implicit solvation at the IPCM(MP2/6-31G**)/RHF/6-31G* level (Table 3).

Results and Discussion

Structures of Substrates and Products. We only considered the most stable conformers of cations **6**–**9** in the present study, and the optimized structures of **6a**, **7a**, **8b-Sg**, and **9a-Sg** are shown in Figure 1. There exists the possibility for conformers about the C5–N bond, and we denote these as **a**- and **b**-isomers. The **a**-structures feature parallel alignment of the ketene moiety and the (NCN)H fragments. Our previous studies showed an **a**-preference for the methyl-substituted cations **6** and **7** (42). For **8** and **9**, various MOM conformations were considered in addition to the choice of C5–N bond conformation (**a** vs **b**). With respect to the rotation about the glycosidic C–N bond, we considered syn (S) and anti (A) conformations. The S and A structures were realized with two additional conformations with respect to the C–O bond of the MOM group, and these included one gauche conformation (g) and one s-trans conformation (st). We showed that the most stable cyano-*N* protonated cation **8** is **8b-Sg** with its through-space electrostatic attraction between the MOM O-atom and the protonated cyanoimine fragment. As to the imino-*N* protonated cation **9**, conformer **9a-Sg** is best because of hydrogen bonding with the MOM O-atom (42).

The structures of the primary reaction products **10** and **11** are shown in Figure 2. Compounds **10** and **11** are tautomers of **1**, and the **a**- and **b**-isomers of **1** also are shown in Figure 2. Tautomerization energies are listed

Table 2. Relative Energies and Relative Gibbs Free Energies^a

process	RHF		MP2		CCSD		IPCM	
	ΔE_{rel}	ΔG_{rel}						
1 → 10b	12.3	10.8	8.5	6.9	11.2	9.6	17.1	15.5
1a → 11a	5.8	5.0	5.0	4.2	5.1	4.3	6.4	5.6
1b → 11b	10.4	9.4	9.0	8.0	9.1	8.1	7.3	6.2
10b → 11b	-1.9	-1.4	0.6	1.1	-2.0	-1.5	-9.8	-9.3
6a → 10b + 12	110.0	95.3	129.1	114.4	124.7	110.0		
7a → 11a + 12	99.8	83.1	119.6	103.0	116.0	99.4		
8b-Sg → 10b + 13	53.6	38.3	62.6	47.3	59.3	44.0	46.5	31.3
9a-Sg → 11a + 13	45.8	28.6	56.0	38.8	53.3	36.1	35.0	17.9
12 + H ₂ O → 14	-61.3	-45.8	-77.3	-61.9	-74.2	-58.8		
13 + H ₂ O → 15	-18.5	-7.7	-20.5	-9.6	-19.8	-8.9	-8.4	2.4
6a + H ₂ O → 10b + 14	48.7	49.5	51.8	52.6	50.4	51.2		
7a + H ₂ O → 11a + 14	38.5	37.3	42.3	41.1	41.8	40.6		
8b-Sg + H ₂ O → 10b + 15	35.0	30.6	42.1	37.7	39.5	35.1	38.1	33.7
9a-Sg + H ₂ O → 11a + 15	27.3	21.0	35.5	29.2	33.5	27.2	26.6	20.3
6a + H ₂ O → 16	-10.3	0.0	-13.7	-3.4	-12.9	-2.6		
7a + H ₂ O → 17	-11.8	-1.8	-14.1	-4.1	-13.7	-3.6		
8b-Sg + H ₂ O → 18	-16.5	-5.7	-18.4	-7.6	-18.0	-7.2	-5.5	5.3
9a-Sg + H ₂ O → 19	-15.5	-4.4	-19.1	-8.0	-18.0	-6.9	-9.3	1.8
10b + 14 → 20	-24.3	-12.2	-31.4	-19.3	-29.4	-17.3		
11a + 14 → 21	-5.4	4.0	-8.5	1.0	-7.7	1.8		
10b + 15 → 22	-15.4	-2.2	-21.3	-8.1	-19.7	-6.5	-11.0	2.2
10b + 15 → 23	-8.5	4.0	-13.8	-1.3	-12.7	-0.2	-7.1	5.4
16 → 20	34.7	37.3	34.1	36.7	33.9	36.5		
17 → 21	44.9	43.1	47.9	46.1	47.7	46.0		
18 → 22	36.1	34.1	39.3	37.3	37.9	35.9	32.7	30.7
19 → 23	34.2	29.4	40.8	35.9	38.9	34.0	28.8	23.9
E_{A} (16 → 24)	51.2	51.3	51.4	51.6	51.2	51.3		
E_{A} (17 → 25)	49.7	46.8	52.0	49.1	51.7	48.9		
E_{A} (18 → 26)	37.2	33.6	42.0	38.4	40.3	36.7	38.0	34.5
E_{A} (19 → 27)	35.7	31.4	42.2	39.0	40.3	36.1	38.5	34.3

^a Relative energies (ΔE_{rel}) and relative free energies (ΔG_{rel}) are in kcal/mol.

Table 3. Natural Charges

	MP2(full)/6-31G**/RHF/6-31G*					IPCM(MP2(full)/6-31G**)/RHF/6-31G*					
	1a	1b	10b	11a	11b	1a	1b	10b	11a	11b	
ketene											
O	-0.280	-0.302	-0.306	-0.285	-0.313	O	-0.291	-0.295	-0.289	-0.283	-0.292
C	0.777	0.790	0.807	0.789	0.775	C	0.812	0.841	0.840	0.814	0.826
CO	0.497	0.488	0.501	0.504	0.462	CO	0.521	0.546	0.551	0.531	0.534
cyanoimine											
N(CN)	-0.378	-0.378	-0.650	-0.329	-0.314	N(CN)	-0.485	-0.476	-0.647	-0.414	-0.417
C	0.375	0.374	0.654	0.410	0.429	C	0.445	0.436	0.674	0.472	0.496
N	-0.571	-0.576	-0.544	-0.669	-0.675	N	-0.623	-0.639	-0.568	-0.666	-0.670
H			0.428	0.472	0.452	H			0.426	0.505	0.488
S	-0.574	-0.580	-0.112	-0.116	-0.108	S	-0.663	-0.679	-0.115	-0.103	-0.103
$\Sigma(\text{NCN})$	-0.574	-0.580	-0.540	-0.588	-0.560	$\Sigma(\text{NCN})$	-0.663	-0.679	-0.541	-0.608	-0.591
$\Sigma(\text{CN}_{\text{term}})$	-0.003	-0.004	0.004	0.081	0.115	$\Sigma(\text{CN}_{\text{term}})$	-0.040	-0.040	0.027	0.058	0.079
$\Sigma(\text{CN}_{\text{cent}})$	-0.196	-0.202	0.110	-0.259	-0.246	$\Sigma(\text{CN}_{\text{cent}})$	-0.178	-0.203	0.106	-0.194	-0.174
imidazole											
N1	-0.596	-0.617	-0.482	-0.499	-0.486	N1	-0.585	-0.603	-0.526	-0.533	-0.546
C2	0.206	0.212	0.161	0.167	0.176	C2	0.229	0.228	0.173	0.176	0.177
N3	-0.429	-0.428	-0.440	-0.439	-0.439	N3	-0.460	-0.461	-0.474	-0.478	-0.479
C4	-0.232	-0.217	-0.209	-0.226	-0.224	C4	-0.241	-0.225	-0.222	-0.237	-0.235
C5	0.424	0.433	0.353	0.378	0.386	C5	0.451	0.455	0.376	0.406	0.416
H	0.241	0.242	0.228	0.232	0.234	H	0.261	0.257	0.236	0.240	0.235
H(NH)	0.460	0.466				H(NH)	0.485	0.481			
S	0.074	0.091	-0.389	-0.387	-0.353	S	0.140	0.132	-0.437	-0.426	-0.432

in Table 2. Attempts to locate the **a**-isomer of **10** in C_1 symmetry afforded the **b**-isomer. For **1** and **11**, both the **a**- and the **b**-isomers exist, and they are nearly isoenergetic for **1**, while the **a**-isomer preference of **11** is about 4 kcal/mol. The intrinsic tautomer stabilities are best compared with the **b**-structures in the absence of complicating through-space interactions between the NCN and the CO fragments. Tautomer **1** is significantly more stable than **10** or **11** by more than 8 kcal/mol, and among the fulvene type systems **10** and **11**, there is a preference of 1–2 kcal/mol for **11**.

The structures of methyl cation **12**, methoxymethyl cation **13**, and their hydrated derivatives **14** and **15** are shown in Figure 3. Ion **14** features a short C–O bond length (1.511 Å), and it is best regarded as a protonated methanol. In contrast, the C–O distance in the hydrated methoxymethyl cation **15** is very long (2.304 Å), and **15** is recognized as a water-solvated oxo-stabilized carbonium ion. The association of carbonium ions R^+ with n -donors produces either covalently bound adducts (e.g., $R-OH_2^+$) or electrostatically bound cluster adducts (e.g., $H_2O \cdots R^+$). The addition of CH_3^+ , $C_3H_5^+$, $sec-C_3H_7^+$, and

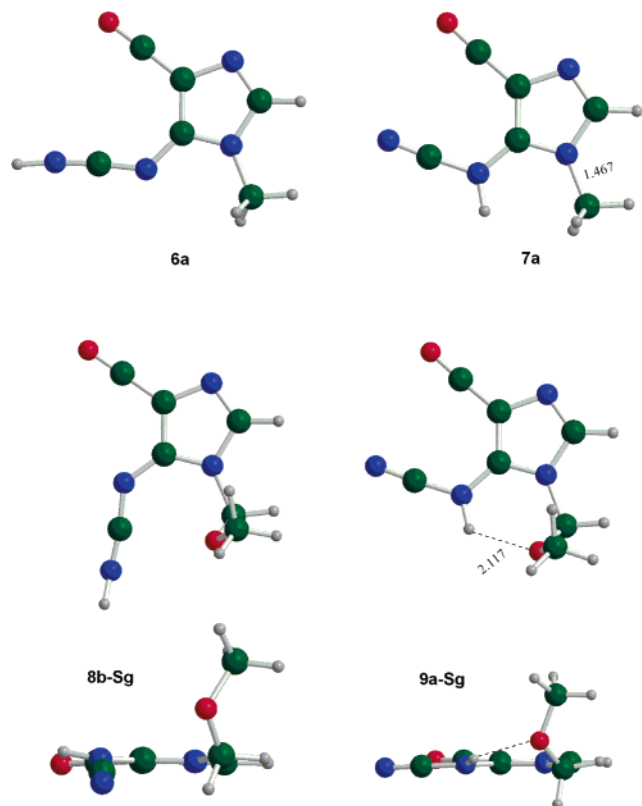


Figure 1. Cyano-*N* protonated cations **6a** (R = Me) and **8b-Sg** (R = MOM) and imino-*N* protonated cations **7a** (R = Me) and **9a-Sg** (R = MOM).

Ⓜ 3D rotatable images of cyano-*N* protonated cations Ⓜ **6a** (R = Me) and Ⓜ **8b-Sg** (R = MOM) and imino-*N* protonated cations Ⓜ **7a** (R = Me) and Ⓜ **9a-Sg** (R = MOM) are available.

$t\text{-C}_4\text{H}_9^+$ to H_2O (51), NH_3 , or alkylamines (52) and HCN or MeCN (53) produces protonated alcohols, amines, and cyanides or isocyanides, respectively, while the addition of H_2O or MeOH to oxocarbenium ions, such as $\text{CH}_3\text{CH}^+(\text{OCH}_3)$ and $(\text{CH}_3)_2\text{C}^+(\text{OCH}_3)$, produces cluster adducts rather than protonated acetals or hemiacetals because the incipient covalent bond is weakened due to the stabilization of the ions (54, 55).

Electron Density Analysis of 5-Cyanoimino-4-oxomethylene-4,5-dihydroimidazoles and the Tautomeric Imidazol-4-ylidenemethanones. Nonzwitterionic Lewis structures of the tautomers **1**, **10**, and **11** are shown in the center row of Scheme 4. These nonzwitterionic Lewis structures do not provide an aromatic system to any one of the tautomers, and instead, they ascribe *ortho*-quinoid electronic structures (5,6-dimethylene-cyclohexa-1,3-diene-type) to **1** and fulvene-like electron densities to **10** and **11**. Hence, the actual electron density distributions should result from attempts to achieve an aromatic imidazole system, and this leads to distinctly different electronic structure types for **1** and for **10** and **11**, respectively. To provide evidence for this hypothesis, electron density analyses were carried out for 5-cyanoimino-4-oxomethylene-4,5-dihydroimidazoles **1a,b**, *N*-[4-(oxomethylene)-imidazol-5-yl]carbodiimide **10b**, and *N*-[4-(oxomethylene)-imidazol-5-yl]-cyanamides **11a,b**, and the results are summarized in Table 3.

We discussed the electronic structure of *N*-methoxymethyl-5-cyanoimino-4-oxomethylene-4,5-dihydroimidazole (**3**) (42), and **1** exhibits similar electronic features. About one-half of a positive charge is localized

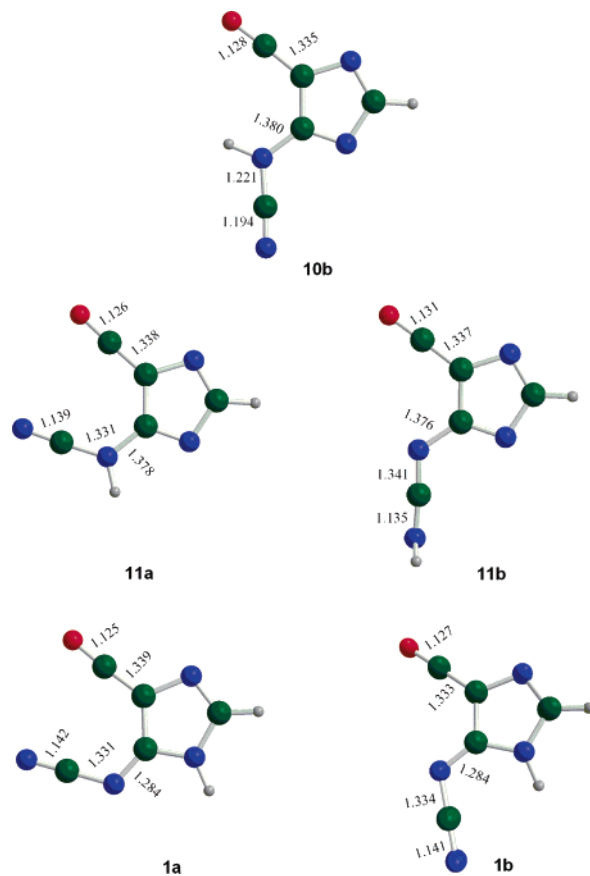


Figure 2. *N*-[4-(Oxomethylene)-imidazol-5-yl]carbodiimide (**10b**) and *N*-[4-(oxomethylene)-imidazol-5-yl]cyanamide (**11**), tautomers of 5-cyanoimino-4-oxomethylene-4,5-dihydroimidazole (**1**).

Ⓜ 3D rotatable images of *N*-[4-(oxomethylene)imidazol-5-yl]carbodiimide Ⓜ **10b** and isomeric *N*-[4-(oxomethylene)imidazol-5-yl]cyanamides Ⓜ **11a** and Ⓜ **11b** are available.

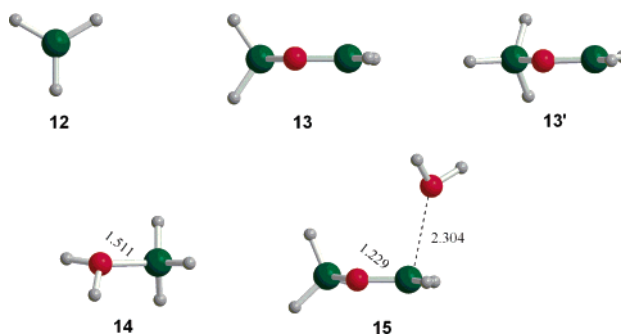
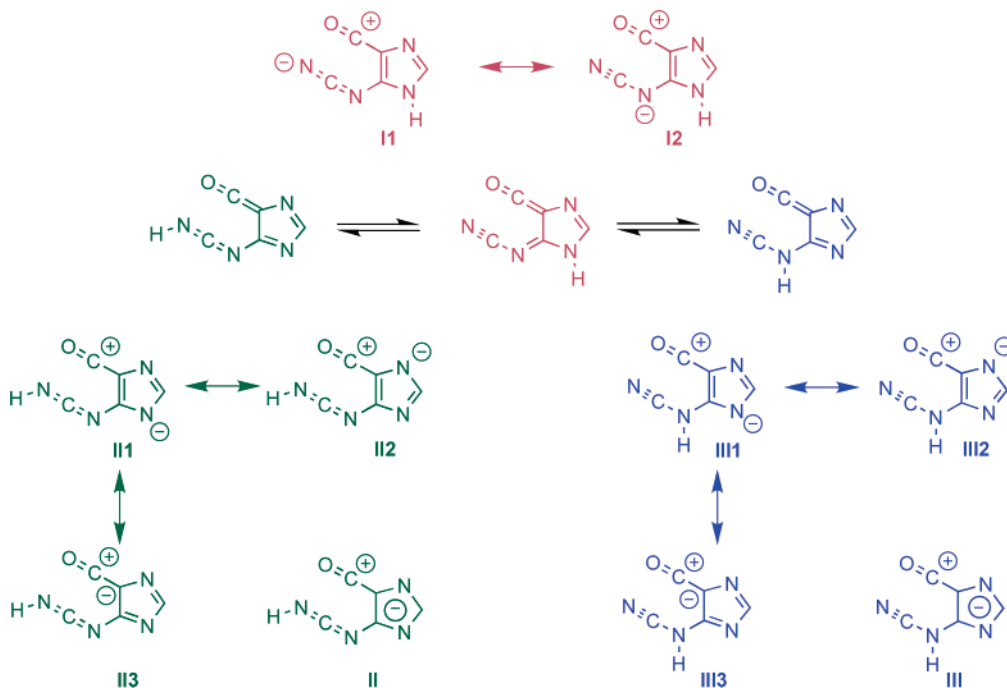


Figure 3. Methyl and methoxymethyl cations **12** and **13** and their water aggregates **14** and **15**. Two C_s conformations of **13** were optimized as follows: *cis*-ip **13** and *trans*-ip **13'**. The vibrational analysis revealed that the former is a minimum while the latter is a transition state.

Ⓜ 3D rotatable images of methyl and methoxymethyl cations Ⓜ **12** and Ⓜ **13** and their water aggregates Ⓜ **14** and Ⓜ **15** are available. Two C_s conformations for the methoxymethyl cation were optimized, *cis*-ip Ⓜ **13** and *trans*-ip Ⓜ **13'**; these 3D rotatable images are also available. The vibrational analysis revealed that the former is a minimum while the latter is a transition state.

on the CO fragment, and one-half of a negative charge is localized on the NCN fragment. Molecules **1** and **3** feature a strong vicinal push (oxomethylene)–pull (cyanoimino) pattern that contributes to resonance forms **11** and **12** with aromatic imidazoles and 4-acylium and

Scheme 4. Electronic Structures of 5-Cyanoimino-4-oxomethylene-4,5-dihydroimidazole (1), *N*-[4-(Oxomethylene)-imidazol-5-yl]carbodiimide (10), and *N*-[4-(Oxomethylene)-imidazol-5-yl]cyanamide (11)



5-cyanoamido groups (Scheme 4). The C4–C5 bond remains highly polarized in this donor–acceptor arrangement. In **10** and **11**, again about one-half of a positive charge is present on the CO fragment. In contrast to **1** and **3**, however, the one-half negative charge remains on the imidazole ring. Our results indicate that the resonance hybrids **II** and **III** are the best representations of the electronic structures of these cations. The heterofulvenes **10** and **11** clearly show features analogous to fulvene (*56*) in that π -electron density is shifted from the exocyclic bond C=C double bond to achieve an aromatic five-membered ring system.

The NCN fragment is highly quadrupolar in the sense N(–)–C(+)-N(–) in all cases. However, the NCN fragments differ greatly in **1** and **3** as compared to the tautomers **10** and **11**. In **1** and **3**, the NCN fragment is overall negative, and there is an electrostatic attraction between it and the acylium group. In contrast, this kind of attraction is much reduced in **10** and **11** because the HNCN fragment is almost neutral. The NCN carbon atom of **10** carries a notably higher positive charge than in the other tautomers; this feature might cause the instability of **10a** type structures to avoid proximity to the acylium group.

Reaction Energy Diagrams for the S_N1 Reactions.

The first step involves heterolysis to form the neutral compounds derivatives **10** or **11** and the respective methyl or methoxymethyl cations **12** or **13** (Scheme 2). The second step involves the addition of water to cations **12** or **13** to form the hydrated complexes **14** or **15**, respectively. The reaction energy diagrams are shown to scale in Scheme 5.

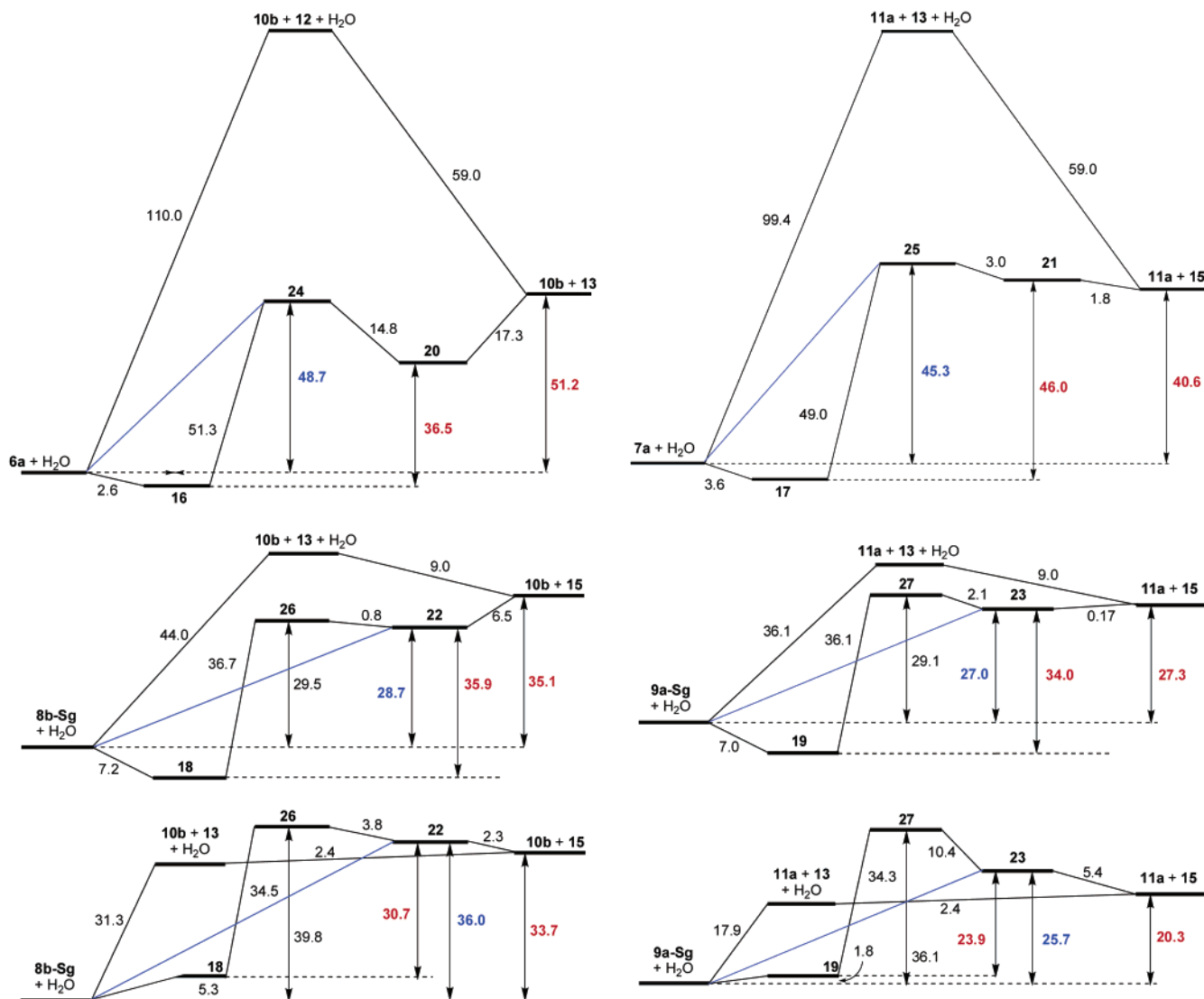
The reaction energy for the first step is drastically lower for MOM-substituted cations **8b-Sg** (44.0 kcal/mol) and **9a-Sg** (36.1 kcal/mol), respectively, than the Me-substituted cations **6a** (110.0 kcal/mol) and **7a** (99.4 kcal/mol), respectively. This huge difference is the result of the methoxy-stabilization of the carbenium ion **13**, and

it is for this reason that one must consider the MOM systems to model “deglycation”. There is a second and less obvious reason, and it concerns the significant differences with which different nucleophiles bind to a given electrophile. The water addition to methyl cation **12** is 50 kcal/mol more exothermic than the water addition to the methoxymethyl cation **13**! This large binding difference is due to covalent bond formation between water and **12** as compared to only weak electrostatic complex formation between water and **13**. The S_N reaction of the MOM system is favored because of the first MOM effect (O-stabilized cation) and in spite of the second MOM effect (low cation–water affinity). The overall reaction energies for **8b-Sg** (35.1 kcal/mol) and **9a-Sg** (27.2 kcal/mol) are about 15 kcal/mol less endothermic than for **6a** (51.2 kcal/mol) and **7a** (40.6 kcal/mol). The reaction of the imino-*N* protonated cations **7a** and **9a-Sg** are less endothermic than those of the cyano-*N* protonated cations **6a** and **8b-Sg** because the former results in the more stable **11a** as compared to **10b**.

Bimolecular Reaction. For the discussion of the bimolecular processes of **6a**, **7a**, **8b-Sg**, and **9a-Sg**, respectively, we considered the corresponding precoordination complexes **16–19**, the postcoordination complexes **20–22**, and the reaction transition state structures **23–26**. All of these structures were located, and they are shown in Figures 4–7.

Precoordination. Complexation of **6a**, **7a**, **8b-Sg**, and **9a-Sg** with water affords the corresponding precoordination complexes **16–19**, respectively. In **16** and **17**, the water coordinates mostly to the C2–H, a known acidic position, and to a lesser degree also to the slightly positively charged Me-hydrogen. All attempts to locate similar precoordination complexes for the MOM systems resulted in the water being moved to its position in **18** and **19**, respectively. Hydrogen bond formation between the water–O and the NCN-attached H-atom clearly is the most important intermolecular interaction with short

Scheme 5. Potential Energy Diagrams for the S_N1 and S_N2 Dealkylation Pathways of Cations 6a and 7a (Top), 8b-Sg, and 9a-Sg (Center and Bottom, Bottom Diagrams Include Solvation)



H-bonding contacts ($<1.8 \text{ \AA}$). Hydrogen bonding between the water-H and the MOM O-atom occurs as a second motif and only if permitted by the dominant H-bonding motif. Complexes **16**–**19** are bound by 2.6, 3.6, 7.2, and 7.0 kcal/mol. The greater stabilities of **18** and **19** are attributed to the stronger H₂O⋯HN hydrogen bonds as compared to the H₂O⋯HC(2) interactions, respectively.

The structures of the precoordination complexes **16** and **17** position the water well to engage in nucleophilic backside attack, and the weak H₂O⋯HC(2) interaction is easily abandoned in the process. The structural rearrangements are more complex for the reactions of **18** and **19**. In the case of **18**, the H₂O⋯HN hydrogen bond is converted into an HOH⋯N(H) hydrogen bond as the water engages in nucleophilic attack. As to **19**, the H₂O⋯HN hydrogen bond is maintained, and the repositioning serves to orient the second water-O lone pair for the nucleophilic attack.

Postcoordination. The optimized postcoordination complexes **20**–**23** are shown to the right in Figures 4–7, and they feature **10b** or **11a** bound to **14** or **15**. Attempts to locate a postcoordination complex **20** containing **10a** failed and led to **20** containing **10b**. This was not unexpected since there is no **10a** conformer for free **10**

(vide supra) and the preference for **10b** should only be enhanced in **20** as it allows for H-bonding between the protonated methanol and the NH nitrogen of **10b**. On the other hand, there does exist a postcoordination complex **21** that contains **11a** (**57**).

The postcoordination complex **22** contains **10b**, and it is similar to **20** in that there is a hydrogen bond formed between the water (donor) and the carbodiimide (N acceptor). Yet, the binding energies differ greatly, and they are 17.3 kcal/mol for **20** and 6.5 kcal/mol for **22**. The Me–HOH⋯NH hydrogen bond is the only intermolecular contact in **20**, and it is a strong hydrogen bond because the H-bond donor is part of a cation (**58**). In **22**, there are two weak intermolecular interactions between **10b** and the H₂O⋯CH₂OMe electrostatic complex, the normal HOH⋯NH hydrogen bond, and the less frequently seen N⋯HC contact between the heterocycle and a CH bond of the methoxymethyl cation (**59**).

Postcoordination complexes **21** and **23** contain **11a**, and the intermolecular interactions differ markedly. The only way to engage the NCNH fragment of **11a** in H-bonding requires NH to be the donor. The O-atom of protonated methanol is not a good donor, and no H-bonding occurs. In **23**, however, the water of the H₂O⋯CH₂OMe electro-

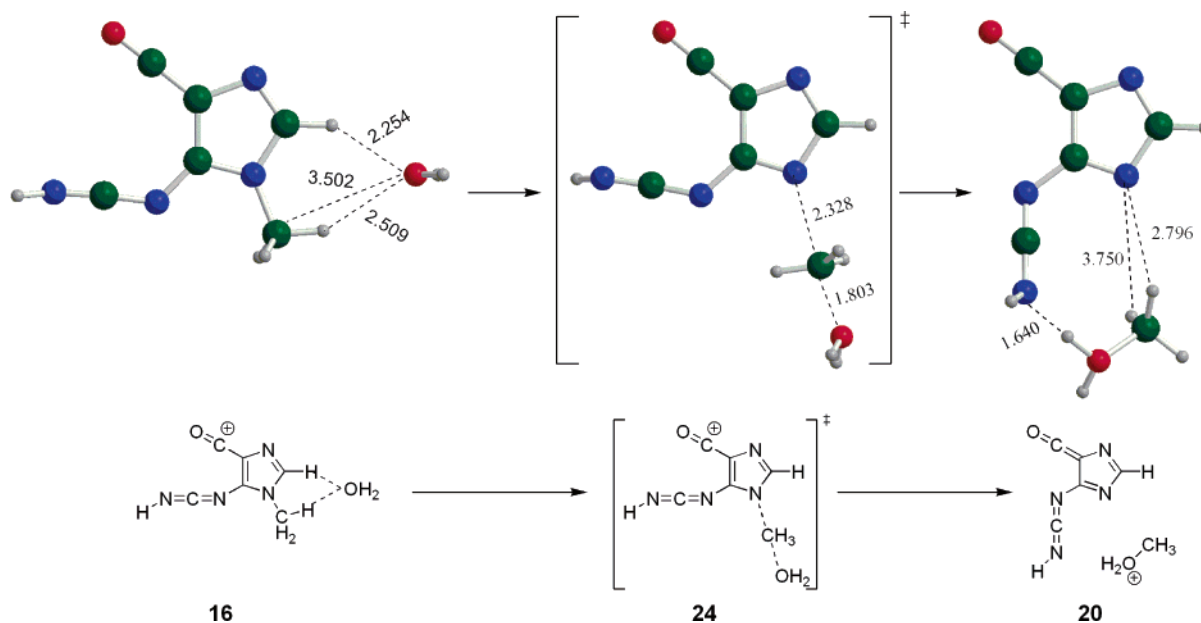


Figure 4. Precoordination complex **16**, transition state **24** (transition state vector), and postcoordination complex **20** for the demethylation of **6a** ($R = \text{Me}$).

Ⓜ 3D rotatable images of precoordination complex Ⓜ **16**, transition state Ⓜ **24** (Ⓜ transition vector animation), and postcoordination complex Ⓜ **20** for the demethylation of Ⓜ **6a** ($R = \text{Me}$) are available.

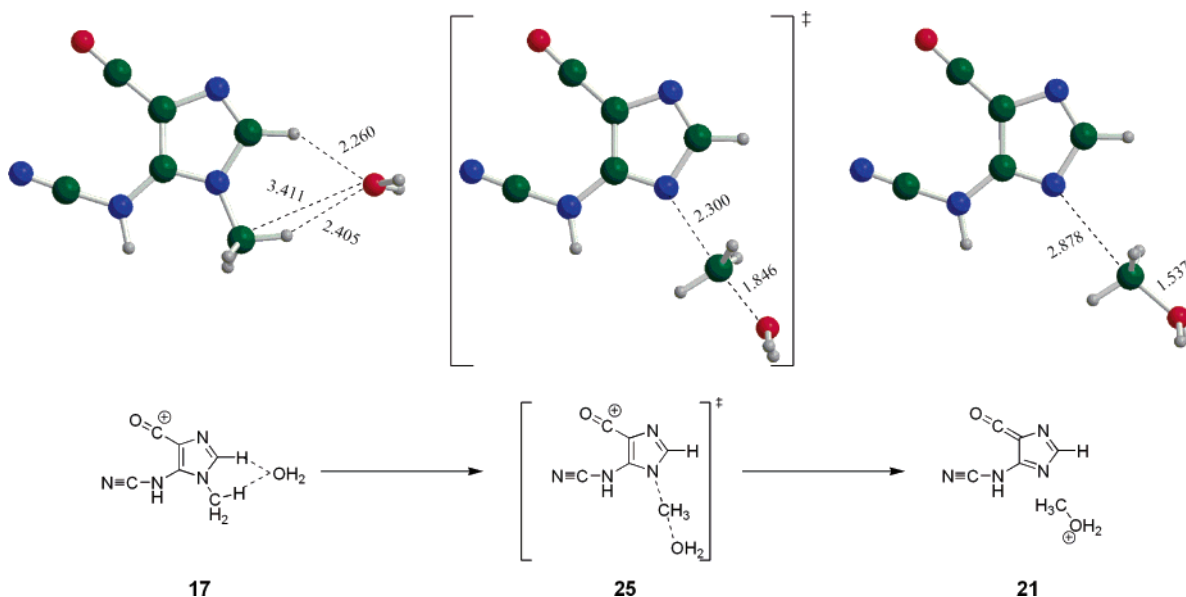


Figure 5. Precoordination complex **17**, transition state **25** (transition state vector), and postcoordination complex **21** for the demethylation of **7a** ($R = \text{Me}$).

Ⓜ 3D rotatable images of precoordination complex Ⓜ **17**, transition state Ⓜ **25** (Ⓜ transition vector animation), and postcoordination complex Ⓜ **21** for the demethylation of Ⓜ **7a** ($R = \text{Me}$) are available.

static complex can form a hydrogen bond with NH, and in addition, an $\text{N}\cdots\text{HC}$ contact occurs between the heterocycle and a CH bond of the methoxymethyl cation. Note that the intermolecular bonding situation is similar in **22** and **23**, but water functions in different ways in its H-bonds.

The complexes **21** and **23** are bound well with respect to the separated products as far as the binding energy ΔE_{rel} is concerned. However, these binding energies are too small to compensate for the entropic advantages of dissociation. The schemes are based on ΔG_{rel} data, and **21** and **23**, respectively, actually are slightly above or isoenergetic relative to the free products.

The reaction energies for the $\text{S}_{\text{N}}2$ dealkylation from precoordination complex to postcoordination complex are 36.5 and 46.0 kcal/mol, respectively, for the reactions of **6a** and **7a**. The reaction becomes less endothermic for **6a** but more endothermic for **7a**. For the MOM systems, the reaction energies are 36.0 and 34.0 kcal/mol, respectively, for cations **8b-Sg** and **9a-Sg**. Again, pre- and postcoordination do not reduce the reaction energy; the complexations leave the reaction energy about the same for the reaction of **8b**, and they render the **9a** reaction a lot more endothermic.

$\text{S}_{\text{N}}2$ Reaction Transition State Structures. The reaction transition state structures **24** and **25** convert **16**

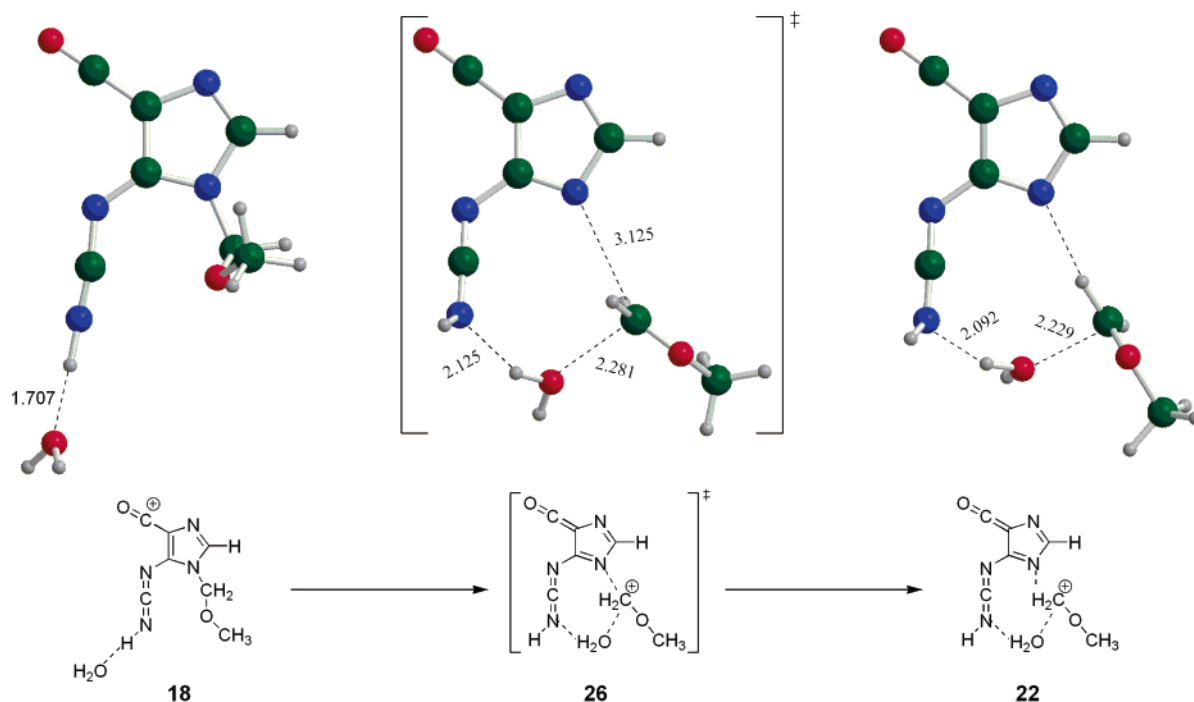


Figure 6. Precoordination complex **18** and postcoordination complex **22** for the dealkylation of **8b-Sg** ($R = \text{MOM}$). The transition state structure **26** (transition vector animation) is in the S_N transition state region and features complete C–N bond heterolysis.

3D rotatable images of precoordination complex **18** and postcoordination complex **22** for the dealkylation of **8b-Sg** ($R = \text{MOM}$) are available. The transition state structure **26** (transition vector animation) is in the transition state region of the S_N process and features complete C–N bond heterolysis.

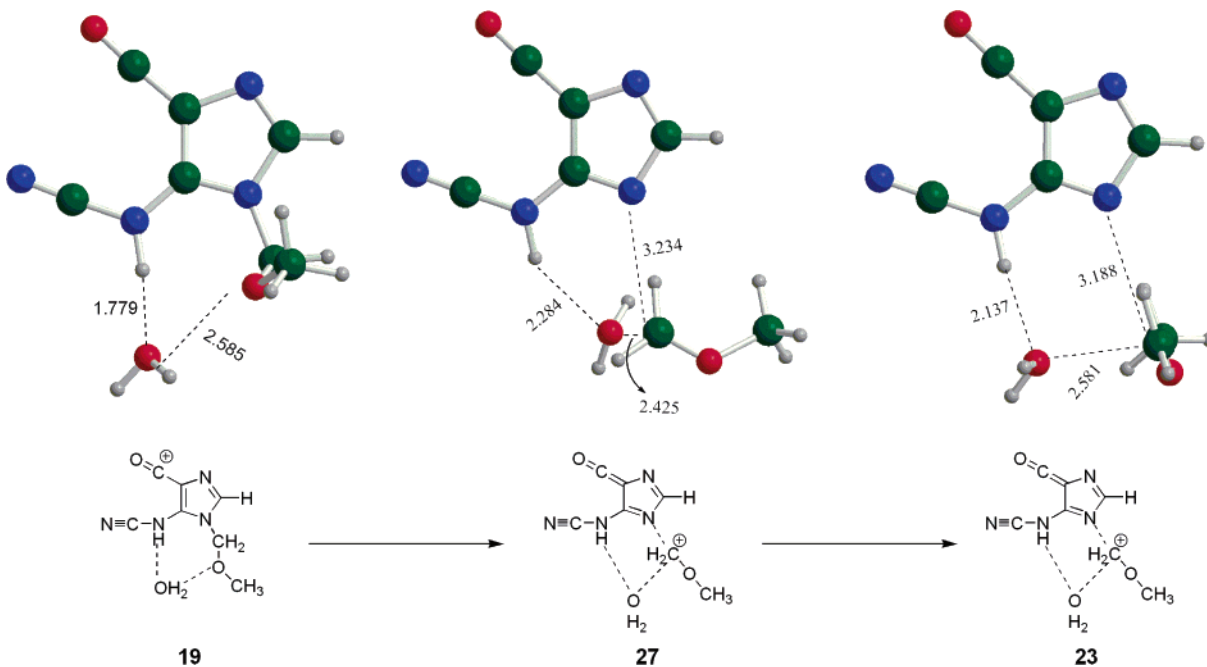


Figure 7. Precoordination complex **19** and postcoordination complex **23** for the dealkylation of **9a-Sg** ($R = \text{MOM}$). The transition state structure **27** (transition vector animation) is in the transition state region of the S_N process and features complete C–N bond heterolysis.

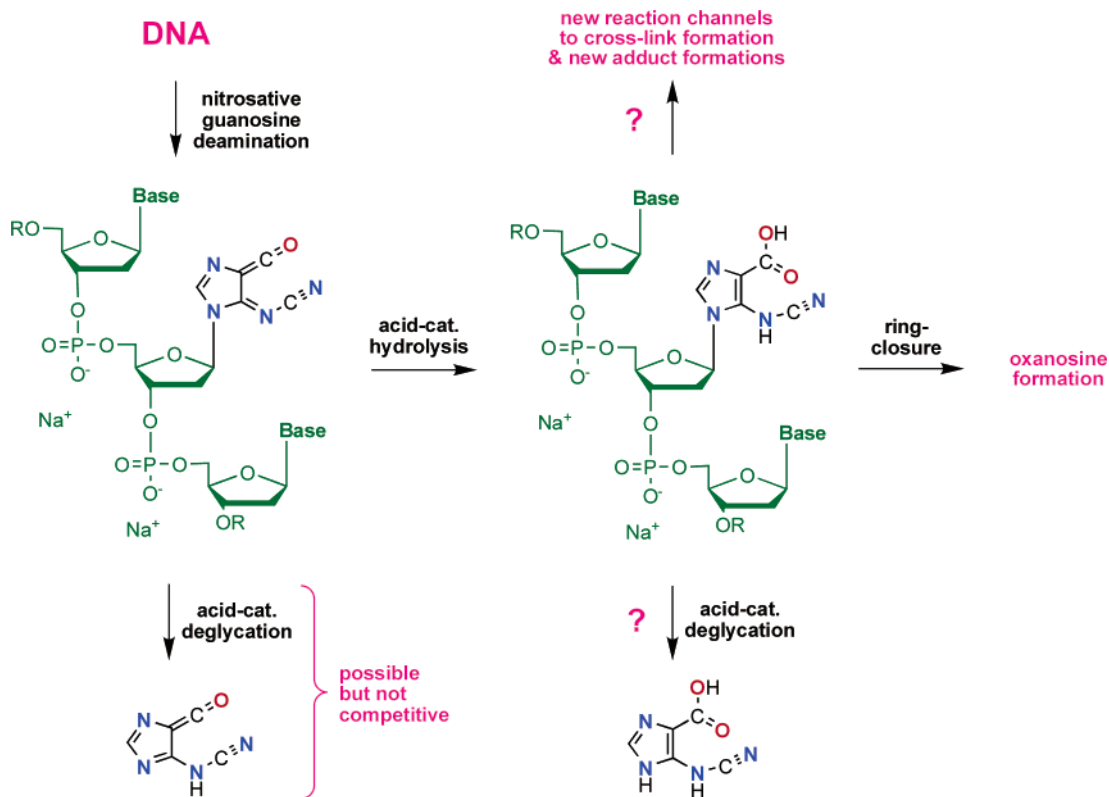
3D rotatable images of precoordination complex **19** and postcoordination complex **23** for the dealkylation of **9a-Sg** ($R = \text{MOM}$) are available. The transition state structure **27** (transition vector animation) is in the transition state region of the S_N process and features complete C–N bond heterolysis.

to **20** and **17** to **21** (Figures 4 and 5), and they are textbook examples of late backside attack S_N2 transition state structures with long C–N and short C–O bonds.

To locate the transition state structures for the reactions of **18** and **19**, the potential energy surfaces were

scanned as a function of the C–N bond length (*35b*). The structures associated with the maxima of the energy profiles were then optimized to the closest transition state structures, and **26** and **27** were obtained in this way. Structures **26** and **27** are transition state structures, and

Scheme 6. Depurination or Deglycation, Depending on Perspective, Might Occur at Various Stages Along the Path to Oxanosine Formation



they are in the transition state region of the bimolecular reaction, but they are not S_N2 transition state structures in the conventional sense. It is the essential feature of both **26** and **27** that the C–N bond is completely broken while the C–O bond is hardly formed. The reaction coordinate also involves a rotational motion, which serves to orient one of the C–H bonds of the developing cationic center toward the N-atom that is being dealkylated. In any case, the main point is the similarity of the products of dissociation and the respective postcoordination complexes. Because there is no strong C–O bond in either of the products, the dealkylation reactions essentially degenerate to C–N bond heterolyses, and they proceed with hardly any nucleophilic assistance.

Activation Barriers for the Hydrolysis Reactions.

The activation barrier for an S_N2 reaction usually is determined as the free energy difference between the precoordination complex and the transition state structure, and this yields activation free energies of 51.3 and 49.0 kcal/mol, respectively, for the reactions of **6a** and **7a**. This procedure assumes that the preordinating water undergoes a unimolecular reaction in the aggregate, and this situation can occur in the gas phase if the precoordination complex is preformed and then allowed to react. A second way for the determination of the activation barrier is based on the difference of the energy of the S_N2 transition state structure and the sum of energies of the free cation and free water. The water molecule might engage in the nucleophilic displacement directly and without prior precoordination. We have recently discussed this direct S_N2 reaction for the hydrolysis of benzenediazonium ion (**60**), and there is a conceptual similarity to a recent discussion of a related S_N2 reaction (**61**). The blue lines in the diagrams in Scheme 5 illustrate this situation, and it is this situation

that most closely mimics the solution chemistry. Hence, our best estimates for the free energies of activation of **6a** and **7a**, respectively, are 48.7 and 45.3 kcal/mol, respectively. The dealkylation reactions of the MOM system present the special case in which the "bimolecular substitution" is reduced to a C–N dissociation and the nucleophilic assistance merely consists of the "solvation" of the formed carbenium ion by a water molecule, an extreme case of an S_N1 -like direct S_N2 reaction. The blue lines in the diagrams on the center in Scheme 5 illustrate this direct S_N2 reaction, and the free energies of activation of **8b-Sg** and **9a-Sg**, respectively, are 28.7 and 27.0 kcal/mol, respectively.

Solvation Effects. The bottom panels of Scheme 5 show the effects of the formal consideration of implicit solvation. The S_N1 reaction now appears lower than the S_N2 path. The gas phase S_N1 reaction invokes complete separation into **10b** or **11a** and **13**. In the actual reaction in solution, however, complete separation is not possible and there is no such thing as a free **13** and its capture of a free water molecule. In solution, water molecules are all around when the C–N bond breaks and the entropy change for the water lucky enough to form the electrostatic complex is nothing like the entropy of association of a formerly free molecule. Clearly, the gas phase S_N1 reaction model is not relevant to the solution chemistry. On the other hand, the structures **22** and **23**, respectively, of the gas phase S_N2 reaction are aggregates of **10b** or **11a**, respectively, with **13** and H_2O . These aggregates do mimic the actual reaction in solution, and the application of the implicit solvation model is justified. With the inclusion of solvation effects, the free energies of activation of **8b-Sg** and **9a-Sg**, respectively, are 36.0 and 25.7 kcal/mol, respectively. Hence, we find a small activation free energy increase of 7.3 kcal/mol for **8b-Sg** and a tiny

decrease of 1.3 kcal/mol for **9a-Sg**. Because ions **8b-Sg** and **9a-Sg** are almost isoenergetic (Table 2) and interconverting fast in solution, this study suggests that an activation free energy of at least 26 kcal/mol is required for dealkylation at N1.

Conclusion

The low activation barriers computed here for the MOM transfer suggest that deglycation could occur at room temperature. Because the addition of water to the acylium moiety is diffusion-controlled, the dealkylation could only occur if the activation barrier were so low as to allow diffusion-controlled dealkylation. The present study demonstrates that the latter clearly is not the case, and we conclude that deglycation cannot compete.

There has never been any full accounting for all of the products of nitrosative guanosine deamination, and one must ask about the fate of all of the guanosine that is not converted into xanthosine, oxanosine, or a dG-to-dG cross-link. If xanthosine is formed entirely (or mostly) by direct nucleophilic heteroaromatic substitution, then there is no reason to assume that any depurination occurred as part of that process. The same applies to any dG-to-dG formed in analogy. Our labeling experiments have shown that oxanosine formation is consistent with the intermediates shown in Scheme 6, that is, deamination leading to 5-cyanoimino-4-oxomethylene-4,5-dihydroimidazole and acid-catalyzed hydrolysis to 5-cyanoaminoimidazole-4-carboxylic acid. The present study suggests that deglycation at the stage of the cyanoimine intermediate is not likely. Further study is necessary to learn whether deglycation might occur at the stage of the cyanoamino intermediate and/or whether the cyanoimine and cyanoamino intermediates might form products that have remained undetected to date.

Acknowledgment. This work was supported by Grant NIGMS GM61027. We thank the University of Missouri–Columbia research computing services for computer time and Drs. G. Springer and L. Sanders for their assistance.

Supporting Information Available: Cartesian coordinates of optimized structures and data for the potential energy surface scans to convert **16** to **20** and **17** to **21**. This material is available free of charge via the Internet at <http://pubs.acs.org>.

References

- Strecker, A. (1861) Untersuchungen über die chemischen Beziehungen zwischen Guanin, Xanthin, Theobromin, Caffein und Kreatinin. *Annals* **118**, 151–177.
- Kossel, A. (1985) Ueber das Adenin. *Berichte* **18**, 1929–1930.
- Kossel, A., and Neumann, A. (1894) Darstellung und Spaltungsproducte der Nucleinsäure. *Z. Physiol. Chem.* **27**, 2215–2222.
- Geiduschek, E. P. (1961) Reversible denaturation of deoxyribonucleic acid (DNA). *Proc. Natl. Acad. Sci. U.S.A.* **47**, 950–955.
- Geiduschek, E. P. (1962) On the factors controlling the reversibility of DNA denaturation. *J. Mol. Biol.* **4**, 467–487.
- Caulfield, J. L., Wishnok, J. S., and Tannenbaum, S. R. (2003) Nitric oxide-induced interstrand cross-links in DNA. *Chem. Res. Toxicol.* **16**, 571–574.
- O'Sullivan, D. A. (1970) Air pollution. *Chem. Eng. News* **48**, 37–41, 45, 46, 50, 54, 55, 57, 58.
- Feldman, P. L., Griffith, O. W., and Stuehr, D. J. (1993) The surprising life of nitric oxide. *Chem. Eng. News* **71**, 26–38.
- Wolff, E. A., and Wasserman, A. E. (1972) Nitrates, nitrites, and nitrosamines. *Science* **177**, 15–19.
- Marnett, L. J. (1996) Nitric oxide: chemical events in toxicity. *Chem. Res. Toxicol.* **9**, 807–808.
- Wink, D. A., Kasprzak, K. S., Maragos, C. M., Elespuru, R. K., Misra, M., Dunams, T. M., Cebula, T. A., Koch, W. H., Andrews, A. W., Allen, J. S., and Keefer, L. K. (1991) DNA deaminating ability and genotoxicity on nitric oxide and its progenitors. *Science* **254**, 1001–1003.
- Kosaka, H., Wisnok, J. S., Miwa, M., Leaf, C. D., and Tannenbaum, S. R. (1989) Nitrosation by stimulated macrophages. Inhibitors, enhancers and substrates. *Carcinogenesis* **10**, 563–566.
- Davis, K. L., Martin, E., Turko, I. V., and Murad, F. (2001) Novel effects of nitric oxide. *Annu. Rev. Pharmacol. Toxicol.* **41**, 203–236.
- Jackson, A. L., and Loeb, L. A. (2001) The contribution of endogenous sources of DNA damage to the multiple mutations in cancer. *Mutat. Res.* **477**, 7–21.
- Kane, J. M., 3rd, Sjeers, L. L., 2nd, Hierholzer, C., Ambs, S., Billiar, T. R., and Posner, M. C. (1997) Chronic hepatitis C virus infection in humans: Induction of hepatic nitric oxide synthase and proposed mechanisms for carcinogenesis. *J. Surg. Res.* **69**, 321–324.
- Grisham, M. B., Jourdeheuil, D., and Wink, D. A. (1999) Physiological chemistry of superoxide and nitric oxide interactions: Implications in DNA damage and repair. *NATO ASI Ser., Ser. A: Life Sci.* **302**, 125–134.
- Ohshima, H., Yermilov, V., Yoshie, Y., and Rubio, J. (1999) DNA damage induced by reactive nitrogen species. *NATO ASI Ser., Ser. A: Life Sci.* **302**, 329–339.
- Nair, J., Ohshima, H., Nair, U. J., and Bartsch, H. (1996) Endogenous formation of nitrosamines and oxidative DNA-damaging agents in tobacco users. *Crit. Rev. Toxicol.* **26**, 149–161.
- Ohshima, H., and Bartsch, H. (1994) Chronic infections and inflammatory processes as cancer risk factors: possible role of nitric oxide in carcinogenesis. *Mutat. Res.* **305**, 253–264.
- Suzuki, T., Yamaoka, R., Nishi, M., Ide, H., and Makino, K. (1996) Isolation and characterization of a novel product, 2'-deoxyoxanosine, from 2'-deoxyguanosine, oligodeoxyribonucleotide, and calf thymus DNA treated by nitrous acid and nitric oxide. *J. Am. Chem. Soc.* **118**, 2515–2516.
- Dong, M., Wang, C., Deen, W. M., and Dedon, P. C. (2003) Absence of 2'-deoxyoxanosine and presence of abasic sites in DNA exposed to nitric oxide at controlled physiological concentrations. *Chem. Res. Toxicol.* **16**, 1044–1055.
- Glaser, R., and Son, M.-S. (1996) Pyrimidine ring opening in the unimolecular dediazonation of guanine diazonium ion. An ab initio theoretical study of the mechanism of nitrosative guanosine deamination. *J. Am. Chem. Soc.* **118**, 10942–10943.
- Glaser, R., Rayat, S., Lewis, M., Son, M.-S., and Meyer, S. (1999) Theoretical studies of DNA base deamination. 2. Ab initio study of DNA base diazonium ions and of their linear, unimolecular dediazonation paths. *J. Am. Chem. Soc.* **121**, 6108–6119.
- Glaser, R., and Lewis, M. (1999) Single- and double-proton-transfer in the aggregate between cytosine and guaninediazonium ion. *Org. Lett.* **1**, 273–276.
- Rayat, S. (2003) Ph.D. Dissertation, University of Missouri–Columbia.
- Qian, M., and Glaser, R. (2004) 5-Cyanoamino-4-imidazolecarboxamide and nitrosative guanine deamination: Experimental evidence for pyrimidine ring-opening during deamination. *J. Am. Chem. Soc.* **126**, 2274–2275.
- Rayat, S., Majumdar, P., Tipton, P., and Glaser, R. (2004) 5-Cyanoimino-4-oxomethylene-4,5-dihydroimidazole and 5-cyanoamino-4-imidazolecarboxylic acid intermediates in nitrosative guanosine deamination. Evidence from (18)O-labeling experiments. *J. Am. Chem. Soc.* Accepted for publication.
- Bothe, E., Dessouki, A. M., and Schulte-Frohlinde, D. (1980) Rate and mechanism of the ketene hydrolysis in aqueous solution. *J. Phys. Chem.* **84**, 3270–3272.
- Duan, X., and Page, M. (1995) Theoretical investigation of competing mechanisms in the thermal unimolecular decomposition of acetic acid and the hydration reaction of ketene. *J. Am. Chem. Soc.* **117**, 5114–5119.
- Kabir, S. H., Saikaly, H. R., and Tidwell, T. (1979) Acid-catalyzed hydration of di-*tert*-butylketene. *J. Am. Chem. Soc.* **101**, 1059–1060.
- Song, B. D., and Jencks, W. P. (1989) Mechanism of solvolysis of substituted benzoyl halides. *J. Am. Chem. Soc.* **111**, 8470–8479.
- Marcus, R. A., and Eyring, H. (1964) Chemical and electrochemical electron-transfer theory. *Annu. Rev. Phys. Chem.* **15**, 155–196.

- (33) Marcus, R. A. (1964) Generalization of the activated complex theory of reaction rates. II. Classical mechanical treatment. *J. Chem. Phys.* **41**, 2624–2633.
- (34) Hoz, S., Basch, H., Wolk, J. L., Hoz, T., and Rozental, E. (1999) Intrinsic barriers in identity S_N2 reactions and the periodic table. *J. Am. Chem. Soc.* **121**, 7724–7725.
- (35) (a) Shaik, S. S., Schlegel, H. B., and Wolfe, S. (1992) *Theoretical Aspects of Physical Organic Chemistry. The S_N2 Mechanism*, John Wiley & Sons, New York. (b) See section 2.4.3.
- (36) Fridgen, T. D., and McMahon, T. B. (2003) Enthalpy barriers for asymmetric S_N2 alkyl cation transfer reactions between neutral and protonated alcohols. *J. Phys. Chem. A* **107**, 668–675.
- (37) Horenstein, B. A., Parkin, D. W., Estupinan, B., and Schramm, V. L. (1991) Transition-state analysis of nucleoside hydrolase from crithidia fasciculata. *Biochemistry* **30**, 10788–10795.
- (38) Lewandowicz, A., and Schramm, V. L. (2004) Transition state analysis for human and *Plasmodium falciparum* purine nucleoside phosphorylases. *Biochemistry* **43**, 1458–1468.
- (39) Farcasiu, D., and Hordsley, J. A. (1980) Ab initio calculations and carbon-13 NMR study on the methoxymethyl cation. *J. Am. Chem. Soc.* **102**, 4906–4911.
- (40) Caserio, M. C., and Kim, J. K. (1982) Ab initio calculations and carbon-13 NMR study on the methoxymethyl cation. *J. Org. Chem.* **47**, 2940–2944.
- (41) Okada, S., Abe, Y., Taniguchi, S., and Yamabe, S. (1987) Kinetic and theoretical study on the ion/molecule reactions of methoxymethyl cation with ammonia. *J. Am. Chem. Soc.* **109**, 295–300.
- (42) Rayat, S., and Glaser, R. (2003) 5-Cyanoimino-4-oxomethylene-dihydroimidazole and nitrosative guanine deamination. A theoretical study of geometries, electronic structures and *N*-protonation. *J. Org. Chem.* **68**, 9882–9892.
- (43) Frisch, M. J., Trucks, G. W., Schlegel, H. B., Scuseria, G. E., Robb, M. A., Cheeseman, J. R., Zakrzewski, V. G., Montgomery, J. A., Jr., Stratmann, R. E., Burant, J. C., Dapprich, S., Millam, J. M., Daniels, A. D., Kudin, K. N., Strain, M. C., Farkas, O., Tomasi, J., Barone, V., Cossi, M., Cammi, R., Mennucci, B., Pomelli, C., Adamo, C., Clifford, S., Ochterski, J., Petersson, G. A., Ayala, P. Y., Cui, Q., Morokuma, K., Malick, D. K., Rabuck, A. D., Raghavachari, K., Foresman, J. B., Cioslowski, J., Ortiz, J. V., Baboul, A. G., Stefanov, B. B., Liu, G., Liashenko, A., Piskorz, P., Komaromi, I., Gomperts, R., Martin, R. L., Fox, D. J., Keith, T., Al-Laham, M. A., Peng, C. Y., Nanayakkara, A., Challacombe, M., Gill, P. M. W., Johnson, B., Chen, W., Wong, M. W., Andres, J. L., Gonzalez, C., Head-Gordon, M., Replogle, E. S., and Pople, J. A. (1998) *Gaussian 98*, Revision A.9, Gaussian, Inc., Pittsburgh, PA.
- (44) Cramer, C. (2002) *Essentials of Computational Chemistry*, Wiley, New York.
- (45) Hehre, W. J., Random, L., Schleyer, P. v. R., and Pople, J. A. (1986) *Ab Initio Molecular Orbital Theory*, John Wiley & Sons, New York.
- (46) Cramer, C. J., and Truhlar, D. (1999) Implicit solvation models: equilibria, structure, spectra, and dynamics. *Chem. Rev.* **99**, 2161–2200.
- (47) Foresman, J. B., Keith, T. A., Wiberg, K. B., Snoonian, J., and Frisch, M. J. (1996) Solvent effects. 5. Influence of cavity shape, truncation of electrostatics, and electron correlation on ab initio reaction field calculations. *J. Phys. Chem.* **100**, 16098–16104.
- (48) Glendening, E. D., Reed, A. E., Carpenter, J. E., and Weinhold, F. *NBO Version 3.1*.
- (49) Glendening, E. D., Badenhop, J. K., and Weinhold, F. (1998) Natural resonance theory. III. Chemical applications. *J. Comput. Chem.* **19**, 628–646.
- (50) Glendening, E. D., and Weinhold, F. (1998) Natural resonance theory. I. General formalism. *J. Comput. Chem.* **19**, 593–609.
- (51) Hiraoka, K., and Kebarle, P. (1977) Condensation reactions involving carbonium ions in the gas phase. Synthesis of protonated acids in gaseous methane containing carbon monoxide and water vapor. *J. Am. Chem. Soc.* **99**, 366–370.
- (52) Meot-Ner, M. (1979) Competitive condensation and proton-transfer reactions. Temperature and pressure effects and the detailed mechanism. *J. Am. Chem. Soc.* **101**, 2389–2395.
- (53) Meot-Ner, M. (1978) Solvation of the proton by hydrogen cyanide and acetonitrile. Condensation of hydrogen cyanide with ions in the gas phase. *J. Am. Chem. Soc.* **100**, 4694–4699.
- (54) Mautner, M., Ross, M. M., and Campana, J. E. (1985) Stable hydrogen-bonded isomers of covalent ions. Association of carbonium ions with *n*-donors. *J. Am. Chem. Soc.* **107**, 4839–4845.
- (55) Glaser, R., and Farmer, D. (1997) The cation-dinitrogen interaction in “benzylidiazonium ion.” Preferential electrostatic complex formation and dinitrogen catalysis of benzyl cation rotational automerization. *Chem. Eur. J.* **3**, 1244–1253.
- (56) Replogle, E. S., Trucks, G. W., and Staley, S. W. (1991) Electron correlation effects on the calculated dipole moments of fulvene and cyclopentadiene. *J. Phys. Chem.* **95**, 6908–6912.
- (57) A postcoordination complex **21** containing **11b** might well exist in which the protonated methanol engaged in H-bonding with the cyano-N atom.
- (58) Desiraju, G. R. (2002) Hydrogen bridges in crystal engineering: Interactions without borders. *Acc. Chem. Res.* **35**, 565–573.
- (59) Hydrogen bonds of neutral donors to electron deficient cations in this way are not well-explored to date. For related studies of ion neutral complexes (INC), see, for example, Aschi, M., Attina, M., and Cacace, F. (1998) Lifetimes of gaseous ion–molecule complexes. *Chem. Eur. J.* **4**, 1535–1541.
- (60) Wu, Z., and Glaser, R. (2004) Ab initio study of the S_N1Ar and S_N2Ar reactions of benzenediazonium ion with water. On the conception of “unimolecular dediazonation” in solvolysis reactions. *J. Am. Chem. Soc.* Accepted for publication.
- (61) Sun, L., Song, K., and Hase, W. L. (2002) A S_N2 reaction that avoids its deep potential energy minimum. *Science* **296**, 875–878.

TX0499416